Computers and Chemical Engineering 35 (2011) 1937–1948

Contents lists available at ScienceDirect

Computers and Chemical Engineering

journal homepage: www.elsevier.com/locate/compchemeng

Modeling and simulation of lithium-ion batteries

Ernesto Martínez-Rosas [a], Ruben Vasquez-Medrano [b], Antonio Flores-Tlacuahuac [b,*]

[a] Facultad de Química, Universidad Nacional Autónoma de México, Ciudad Universitaria, México D.F. 04510, Mexico
[b] Departamento de Ingeniería y Ciencias Químicas, Universidad Iberoamericana, Prolongación Paseo de la Reforma 880, México D.F. 01210, Mexico

ARTICLE INFO

Article history:
Received 26 October 2010
Received in revised form 9 May 2011
Accepted 10 May 2011
Available online 27 May 2011

Lithium-ion batteries
Modeling
Simulation
Energy

ABSTRACT

In this work the dynamic one-dimensional modeling and simulation of Li ion batteries with chemistry $Li_xC_6 - - Li_yMn_2O_4$ is presented. The model used is robust in terms of electrochemical variables prediction rather than only the electrical ones. This enables us to analyze the internal behavior of the battery under different discharge rates. The method of lines (MOL) was used for predicting the behavior from the model without any loss of exactitude for regular geometries. The boundary conditions were modified to achieve a better convergence of the solver. The simulation results were compared to experimental data from the research literature. Some examples of application are also presented that include the simulation for the optimization of design parameters, the evaluation of the behavior of the battery under dynamic discharge rates simulating real simplified conditions of operation and the simulation of the parallel discharge of different capacity pairs of batteries.

1. Introduction

The race for alternative energy sources and green technologies is speeding worldwide, mainly due to global warming and the forecast run out of fossil fuels. However, these are not the only reasons. From an economic profit point of view, there is a growing sector of environmental aware buyers, willing to spend something extra to reduce their impact to the planet. The real concern is that many of these green technologies simply propose to move the CO_2 generation from our vehicles to a power plant. An appropriate solution to prevent CO_2 generation would be to replace internal combustion vehicles with alternative energy sources. Among these sources there are: biofuels, compressed air, electric fuel cells and rechargeable batteries.

There are many options for electric vehicle batteries, each system offers unique features with advantages and disadvantages. The most promising batteries are lithium ion (Li-ion) which provide high energy density (Scrosati & Grache, 2010). However, Li-ion batteries have problems with the sensitivity to the overload that may reduce its life cycle. Other options under study include fuel cells and mechanically rechargeable batteries. In any case, it should be noted that these options do not offer the same amount of energy as fossil fuels do (~40 MJ/kg for fossil fuels versus 1.5–0.25 MJ/kg for fuel cells and advanced batteries respectively (Linden & Reddy, 2002)).

Although EVs were designed and built in the past century, internal combustion (IC) vehicles were the best choice because of low oil prices. Currently there is no power source that equals the capacity of acceleration (power) and range (energy) of the IC engine. Nevertheless, researches are conducted in the hope that a robust system, capable of meeting reasonable acceleration and range capabilities, can displace the IC engine (Cairns & Albertus, 2010). Fuel cells and Li-ion batteries are good alternatives for use in electric vehicles.

Lithium ion batteries where introduced commercially in the 1990s for portable applications such as camcorders and cameras (Ozawa, 1994). They offered a greater capacity than nickel (Ni) batteries for portable devices but their cost was prohibitive for larger application (20,000 kWh) (Cairns & Albertus, 2010). The lithium ion batteries use graphite as the anode while the cathode is a cobalt oxide, the two electrodes are porous. The electrolyte is a mixture of organic solvents and a lithium salt. Different organic compounds are used as electrolytes because lithium is highly reactive in water (Linden & Reddy, 2002). Most common electrolytes include: Dimethyl carbonate (DMC), ethyl methyl carbonate (EMC) and diethyl carbonate (DEC) (Huggins, 2009). In terms of electrodes, several compounds have been proposed since the original LiC_6–$LiCoO_2$ (Broussely & Archdale, 2004; Whittingham, 2004). The use of graphite as the anode material is universally accepted (Chung, Jun, Lee, & Kim, 1999; Michio, 1996; Tran, Spellman, Pekala, Goldberger, & Kinoshita, 1995), while the following compounds: $LiNiO_2$, $LiMn_2O_4$, $LiMn_{1/3}Ni_{1/3}Co_{1/3}O_2$ and $LiFePO_4$ have been used as cathodes (Delmas & Saadoune, 1992; Seung-Taek et al., 2008; Shina, Basak, Kerr, & Cairns, 2008; Wang, Bradhurst, Dou, & Liu, 1998). Li-ion batteries employ very thin (10–30 μm), microporous films to electrically isolate the negative and positive electrodes.

* Corresponding author. Tel.: +52 55 59504074; fax: +52 55 59504074.
E-mail address: antonio.flores@uia.mx (A. Flores-Tlacuahuac).

0098-1354/$ – see front matter © 2011 Elsevier Ltd. All rights reserved.
doi:10.1016/j.compchemeng.2011.05.007

Nomenclature

List of symbols

a	specific interfacial area, m^2/m^3
c	concentration of Li ions in the electrolyte, mol/m^3
C_s	concentration of Li in the electrode, mol/m^3
D	diffusion coefficient of the salt in the electrolyte, m^2/s
D_s	diffusion coefficient of Li in the electrode, m^2/s
F	Faraday's constant, 96,487 C/mol
$f_{\pm}$	activity of the salt in the electrolyte, mol/m^3
$\mathbf{i}_1$	current density in the electrode, A/m^2
$\mathbf{i}_2$	current density in the electrolyte phase, A/m^2
I	total current density, A/m^2
j_{Li}	pore wall flux of Li ions, mol/cm^2 s
$\mathbf{N}$	mass transport flux, mol/m^2
$\mathbf{R}$	reaction term of the mass balance equation, mol/m^3 s
R	gas constant, 8.314 J/mol K
R_f	film resistance, $\Omega\,m^2$
R_s	radius of electrode spherical particle, m
T	temperature of the system
t	time of operation, s
t_+^o	transport number of the positive ion
u^0	open circuit voltage, V

Greek

δ	region width
ε	porosity of the composite electrodes
η	over-potential, V
κ	ionic conductivity of electrolyte, S/m
σ	electronic conductivity of solid matrix, S/m

Index

a	anode
s	separator
c	cathode
T	maximum concentration in intercalation material
0	initial condition

All commercially available liquid electrolyte cells use microporous polyolefin materials as they offer excellent mechanical properties, chemical stability and satisfactory cost. Currently the microporous polyolefin materials are made of polyethylene, polypropylene or laminate of polyethylene and polypropylene (Linden & Reddy, 2002). The separator operates as the solvent for a lithium salt. Properties for different salts and polymer combinations are cited in the literature (Doyle, Fuller, & Newman, 1993).

Lithium ion cells operation is based on a process known as rocking-chair, owing its name to the extraction and intercalation of lithium ions from the electrodes that correspond to the donation and acceptance of electrons respectively (Doyle et al., 1993). The overall charge/discharge cycle is then seen as a swing of lithium ions between electrodes. Intercalation/extraction presents advantages and disadvantages compared to the traditional oxidation/reduction scheme. Intercalation and extraction are topotactic processes of moderate to high reversibility, that present a change in the volume of the host, depending of its nature, which over cycling life leads to degradation of the matrix (Liaw, Jungst, & Nagasubramanian, 2011).

The use of $LiMn_2O_4$ has the advantages of low cost, good stability and adequate specific capacity (120 mAh/g, compared to 140 mAh/g that provides the $LiCoO_2$). In this work, we have chosen to simulate the LiC_6–$LiMn_2O_4$ battery for two main reasons. First, because of its low cost and their appropriate characteristics making it a promising alternative for using in electric vehicles. Secondly, because there are published data for different parameters needed to develop the mathematical model.

A simplified model for this type of battery has been solved analytically by partial differential and algebraic equations, but this model is only valid for a limited set of conditions (Baker, & Verbrugge, 2011). There are also some proposed equivalent circuits for the description of the electrical variables of charge and discharge of the battery but the accuracy of these variables are not robust to describe the electrochemical phenomena (Liaw et al., 2005). On the other hand, different numerical simulation methods have been used to solve models of lithium ion batteries. Approaches to this problem include the linearization of the system using the BAND program (Doyle & Newman, 1996), finite element (Tang, Albertus, & Newmana, 2009) and Newton–Krylov algorithms (Wu, Srinivasan, Xu, & Wang, 2002). With the use of numerical methods it has been possible to solve different models related to batteries. Among these we mention the optimization of the thickness of the electrode (Fuller, Doyle, & Newman, 1994), the performance of batteries with electrodes of complex geometry (Garca & Chiang, 2007) and determining the capacity and discharge rate of batteries (Ning & Popov, 2004.

The contribution of this work lies in formulating and experimentally validating a mathematical model suitable for approaching the design, optimization and control of Li-ion batteries. We used a modified version of the model presented by Doyle and Newman (1996) for the lithium ion battery with chemistry LiC_6–$LiMn_2O_4$. Modifications were made in the boundary conditions to determine the potential of both electrodes and the electrolyte. The original model used flux boundary conditions whereas we transformed some of these conditions to specified values, improving the convergence of the model. The transformation was made based on the fact that the current supplied by each portion of the anode should sum up to the total current. This also applies to the accepted current in the cathode side. We also included a consistent initialization strategy, similar to the one proposed in Boovaragavan and Subramanian (2007), to promote the quick start of the solver used for getting the dynamic and spatial behavior of the battery. The model was solved by the numerical method of lines (MOL) (Schiesser, 1991), which is easier to deploy than the finite element or finite volume especially for systems with regular geometries as the one addressed in the present work.

In the first section we present the mathematical model in detail and modifications from the original model (Doyle & Newman, 1996). Secondly we deal with the reduced version of the model assuming constant and null terms for the LiC_6–$LiMn_2O_4$ chemistry. The next section is the validation of the model where we present the comparison between simulated and experimental data from previous works (Doyle & Newman, 1996). Finally we present some examples of application which include: (1) variation of design parameters for the optimization of battery performance, (2) the dynamic response to a varying rate of discharge and (3) the discharge simulation of different capacity batteries connected in parallel.

2. Mathematical model

The electrochemical system under study has the chemistry Li_xC_6–$Li_yMn_2O_4$. In this type of batteries, electricity is produced by the simultaneous insertion/deinsertion of lithium ion in the porous cathode and anode respectively. Deinsertion process releases electrons that go into the electric circuit, on the other side, these electrons are accepted to cause insertion of lithium ions. Inside the battery, positively charged lithium ions move from the anode

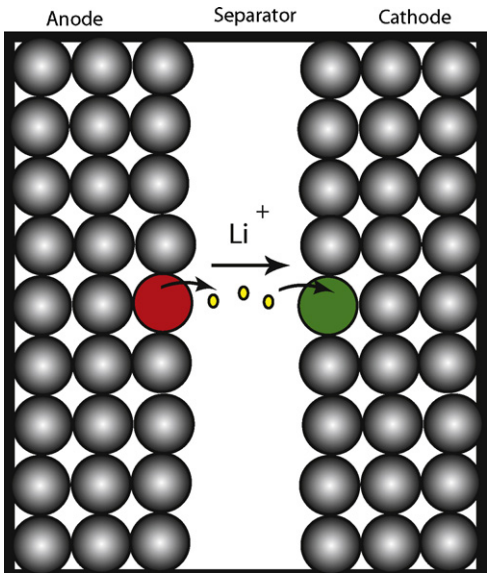

Fig. 1. Li_xC_6-- $Li_yMn_2O_4$ battery.

where they where released towards the cathode where electrons return closing the electric circuit, this process is known as "rocking-chair" because of the overall effect of lithium ions, which move from anode to cathode during discharge and backwards upon charging. Fig. 1 shows a scheme of this system. The model assumes that the active material of both electrodes is spherical and it is supported on an inert material. The electrolyte is $LiPF_6$ in a EC/DMC 2:1 solvent. There is an insertion/deinsertion phenomenon occurring at the electrodes as the charge and discharge processes occur.

The Faradic process deals with everything concerned to the heterogeneous oxidation-reduction reactions and the electric charges involved in this. The formulas governing this process are the normal and modified Ohm's law and the insertion/deinsertion of Li ions into the active materials.

Faraday's laws express the relationship between the insertion/deinsertion of Li-ions into electrodes with the electrical charge flow (all the variables are described in Nomenclature section).

$$\nabla \cdot \mathbf{i}_2 = Faj_{Li} \tag{1}$$

Based on the law of conservation of charge, current density is preserved between the electrode and electrolyte, therefore we obtain the following expression:

$$\nabla \cdot (\mathbf{i}_1 + \mathbf{i}_2) = 0 \tag{2}$$

$$\mathbf{i}_1 + \mathbf{i}_2 = I \tag{3}$$

this provides a relation between Li-ions flux with both current densities:

$$\nabla \cdot \mathbf{i}_1 = -Faj_{Li} \tag{4}$$

$$\nabla \cdot \mathbf{i}_2 = Faj_{Li} \tag{5}$$

The model assumes that both electrodes are porous and non-flat surfaces such as in most common batteries. As mentioned, the model assumes that the active materials are spherical particles supported in the filling material. Moreover, we assume that the solid phase diffusion coefficient is independent of concentration. However, there are some cases wherein they are function of concentration. Therefore, the Li-ion concentration in the active material is simulated via molecular diffusion in spherical coordinates according to the following equation:

$$\frac{\partial C_s}{\partial t} = D_s \left[\frac{\partial^2 C_s}{\partial r^2} + \frac{2}{r} \frac{\partial C_s}{\partial r} \right] \tag{6}$$

Charge and discharge of the battery is only possible in a closed circuit. In the electrodes and the external electrical circuit, electrical current is generated by the flow of electrons, whereas in the electrolyte, the electric current is due to ions flow. In both cases, the electric current is the same. The electrode potential (ϕ_1) is calculated with Ohm's law:

$$\mathbf{i}_1 = -\sigma \nabla \phi_1 \tag{7}$$

In the electrolyte, under the effect of concentration gradients, Ohm's law does not describe accurately the ionic transport of charges. A modification of Ohm's law can be used instead (Doyle & Newman, 1996):

$$\kappa \nabla \phi_2 = -\mathbf{i}_2 - \frac{2\kappa RT}{F} \left(1 + \frac{\partial ln f_{\pm}}{\partial ln c} \right) \left(1 - t_+^o \right) \nabla ln c \tag{8}$$

This equation relates the potential with the local current density. Nevertheless, it is more convenient to relate the potential to the Li ion flux. This can be done by differentiating (in x) the equation of current density:

$$\nabla \cdot \mathbf{i}_2 = \nabla \cdot \left(-\kappa \nabla \phi_2 - \frac{2\kappa RT}{F} \left(1 + \frac{\partial ln f_{\pm}}{\partial ln c} \right) (1 - t_+^o) \nabla ln c \right) \tag{9}$$

Finally we substitute the current density gradient for its equivalent in terms of Li ion flux according to Faraday's laws, leading to the following equations:

$$-\sigma \nabla^2 \phi_1 = -Faj_{Li} \tag{10}$$

$$-\kappa \nabla^2 \phi_2 = Faj_{Li} + \frac{2\kappa RT}{F} \left(1 + \frac{\partial ln f_{\pm}}{\partial ln c} \right) (1 - t_+^o) \nabla^2 ln c \tag{11}$$

On the other hand, when the heterogeneous reaction (electrode/electrolyte interface) is controlled by the activation, the kinetics can be described by the Butler–Vomer equation:

$$j_n = i_o \left\{ \exp\left(\frac{F}{2RT(\eta - u^o)} \right) - \exp\left(\frac{-F}{2RT(\eta - u^o)} \right) \right\} \tag{12}$$

2.1. Mass transport process

Electrolyte is present in the three battery regions (anode, separator and cathode). The mass balance is deduced by the concentrated solution theory (Newman & Thomas-Alyea, 2004) and includes the migration and diffusion effects. The total flux is thus represented by:

$$\mathbf{N}_+^{\text{Total}} = -D \left(1 - \frac{d \ln c_o}{d \ln c} \right) \cdot \nabla c + \frac{\mathbf{i}_2 t_+^o}{F} \tag{13}$$

On the other hand, the reaction term that occurs at the electrodes is expressed as:

$$\mathbf{R} = \frac{a}{\nu_+} (1 - t_+^o) j_{Li} \tag{14}$$

The overall mass balance is:

$$\frac{\partial c}{\partial t} = -\nabla \cdot \mathbf{N} + \mathbf{R} \tag{15}$$

If we substitute the previous definitions in the overall mass balance we have the general formula for the concentration of lithium ions in the electrolyte:

$$\frac{\partial c}{\partial t} = -\nabla \cdot \left(-D \left(1 - \frac{d \ln c_o}{d \ln c} \right) \nabla c + \frac{\mathbf{i}_2 t_+^o}{F} \right) + \frac{a}{\nu_+} (1 - t_+^o) j_{Li} \tag{16}$$

Table 1
Constant and null terms (Doyle & Newman, 1996).

Term	Status	Explanation
t_+^o	Constant	It has been proved that the transport number is a function of the Li-ions concentration in the electrolyte, however there is not reliable data for these dependence
n	Constant	These specific battery and in general all the based in lithium, are restricted to the transference of one electron per atom of reacting Li
ν_+	Constant	The electrolyte used in this battery is dissociated in a 1:1 relation
s_+	Constant	In both anodic and cathodic reactions the Li coefficient is 1
$\frac{d(\ln c_0)}{d(\ln c)}$	Null	This term is neglected due to the lack of experimental data
$\frac{\partial \ln f_\pm}{\partial \ln c}$	Null	This term is neglected due to the lack of experimental data

$$\frac{\partial c}{\partial t} = D\left(1 - \frac{d\ln c_o}{d\ln c}\right)\nabla^2 c - \frac{\boldsymbol{i}_2 \nabla \cdot t_+^o}{F} + \frac{a}{\nu_+}(1 - t_+^o) j_{Li} \quad (17)$$

The previous formula is only valid for the continuous region of the battery i.e. the separator. In order to make it applicable to the electrode regions we have to take into account the porosity of the medium. In this way we obtain a more general formula that is applicable to all three regions (Doyle & Newman, 1996):

$$\epsilon\frac{\partial c}{\partial t} = D\left(1 - \frac{d\ln c_o}{d\ln c}\right)\nabla^2 c - \frac{\boldsymbol{i}_2 \nabla \cdot t_+^o}{F} + \frac{a}{\nu_+}(1 - t_+^o) j_{Li} \quad (18)$$

2.2. Governing equations

Li-ion diffusion in the electrolyte

$$\epsilon\frac{\partial c}{\partial t} = D\left(1 - \frac{d\ln c_o}{d\ln c}\right)\nabla^2 c - \frac{\boldsymbol{i}_2 \nabla \cdot t_+^o}{F} + \frac{a}{\nu_+}(1 - t_+^o) j_{Li} \quad (19)$$

Faraday's laws

$$a j_{Li} = \frac{1}{F}\nabla \cdot \mathbf{i}_2 \quad (20)$$

Ohm's law (electrode)

$$-\sigma\nabla^2\phi_1 = -Fa j_{Li} \quad (21)$$

Modified Ohm's law (electrolyte)

$$-\kappa\nabla^2\phi_2 = Fa j_{Li} + \frac{2\kappa RT}{F}\left(1 + \frac{\partial \ln f_\pm}{\partial \ln c}\right)\left(1 - t_+^o\right)\nabla^2 \ln c \quad (22)$$

Li ion diffusion in the active material

$$\frac{\partial C_s}{\partial t} = D_s\left[\frac{\partial^2 C_s}{\partial r^2} + \frac{2}{r}\frac{\partial C_s}{\partial r}\right] \quad (23)$$

2.3. Simplification

2.3.1. Constant terms

The presented model is general and thorough. However, the model can be simplified by means of the consideration of constant or null terms related to the Li_xC_6−− $Li_yMn_2O_4$ system (Doyle & Newman, 1996). An explanation of these terms is presented in Table 1. Considering the simplification of terms, we can rewrite the governing equations as follows:

- Li ion diffusion in the electrolyte

$$\epsilon\frac{\partial c}{\partial t} = D\nabla^2 c + a(1 - t_+^o) j_{Li} \quad (24)$$

- Modified Ohm's law (electrolyte)

$$-\kappa\nabla^2\phi_2 = Fa j_{Li} + \frac{2\kappa RT}{F}\left(1 - t_+^o\right)\nabla^2 \ln c \quad (25)$$

Eqs. (19)–(23) can be rewritten as follows assuming a single dimension (1D). (For the active material, spherical diffusion occurs only in the r dimension)

- Li-ion diffusion in the electrolyte

$$\epsilon\frac{\partial c}{\partial t} = D\frac{\partial^2 c}{\partial x^2} + a(1 - t_+^o) j_{Li} \quad (26)$$

- Faraday's laws

$$\frac{1}{F}\frac{d\mathbf{i}_2}{dx} = a j_{Li} \quad (27)$$

- Ohm's law (electrode)

$$-\sigma\frac{\partial^2\phi_1}{\partial x^2} = -Fa j_{Li} \quad (28)$$

- Modified Ohm's law (electrolyte)

$$-\kappa\frac{\partial^2\phi_2}{\partial x^2} = Fa j_{Li} + \frac{2\kappa RT}{F}\left(1 - t_+^o\right)\frac{\partial^2 \ln c}{\partial x^2} \quad (29)$$

- Li-ion diffusion in the active material

$$\frac{\partial C_s}{\partial t} = D_s\left[\frac{\partial^2 C_s}{\partial r^2} + \frac{2}{r}\frac{\partial C_s}{\partial r}\right] \quad (30)$$

2.3.2. Dimensionless equations

This model was made dimensionless in the x variable and also in the r coordinate of the spherical particles. The variable change obeys to the following formulas:

$$x^* = \frac{x}{\delta} \quad (31)$$

$$r^* = \frac{r}{R_s} \quad (32)$$

As an example we take the Ohm's law:

$$-\sigma\frac{\partial^2\phi_1}{\partial x^2} = -Fa j_{Li} \quad (33)$$

Applying the dimensionless formula we get:

$$-\sigma\frac{\partial^2\phi_1}{\delta^2\,\partial x^{*2}} = -Fa j_{Li} \quad (34)$$

we can adopt the convention of defining x^* as x to avoid visually overcharging the equations. In this way we have:

$$-\sigma\frac{\partial^2\phi_1}{\delta^2\,\partial x^2} = -Fa j_{Li} \quad (35)$$

When we proceed in the same way for all the equations we have:

- Li-ion diffusion in the electrolyte

$$\epsilon\frac{\partial c}{\partial t} = \frac{D}{\delta^2}\frac{\partial^2 c}{\partial x^2} + a(1 - t_+^o) j_{Li} \quad (36)$$

- Faraday's laws

$$\frac{1}{\delta F}\frac{d\mathbf{i}_2}{dx} = a j_{Li} \quad (37)$$

- Ohm's law (electrode)

$$\frac{-\sigma}{\delta^2}\frac{\partial^2\phi_1}{\partial x^2} = -Fa j_{Li} \quad (38)$$

- Modified Ohm's law (electrolyte)

$$\frac{-\kappa}{\delta^2}\frac{\partial^2\phi_2}{\partial x^2} = Fa j_{Li} + \frac{2\kappa RT}{\delta^2 F}\left(1 - t_+^o\right)\frac{\partial^2 \ln c}{\partial x^2} \quad (39)$$

- Li-ion diffusion in the active material

$$\frac{\partial C_s}{\partial t} = \frac{D_s}{R_s^2}\left[\frac{\partial^2 C_s}{\partial r^2} + \frac{2}{r}\frac{\partial C_s}{\partial r}\right] \tag{40}$$

2.4. Boundary conditions

This model presents three regions in the x dimension and two regions in the r sub-dimension. In the next section we shall discuss the boundary conditions of all equations between regions.

- Li-ion diffusion in the electrolyte Diffusion takes place in the three regions of the cell (anode, separator and cathode as seen in Fig. 1). Current collectors present an impermeable wall to the electrolyte, therefore the Li-ion flux is null in these boundaries. The interfaces of the three regions show a continuity condition that is expressed as an equality of the mass fluxes on both sides of the interface. Mathematically we have:

  In the current collectors

$$\left.\frac{\partial c}{\partial x}\right|_{x=0} = 0 \tag{41}$$

$$\left.\frac{\partial c}{\partial x}\right|_{x=L} = 0 \tag{42}$$

  At the interfaces:

$$\left.\frac{\partial c}{\partial x}\right|_{x+=\delta_a} = \left.\frac{\partial c}{\partial x}\right|_{x-=\delta_a} \tag{43}$$

$$\left.\frac{\partial c}{\partial x}\right|_{x+=\delta_a+\delta_s} = \left.\frac{\partial c}{\partial x}\right|_{x-=\delta_a+\delta_s} \tag{44}$$

- Li-ion diffusion in the active material

$$\left.\frac{\partial C_s}{\partial r}\right|_{r=0} = 0 \tag{45}$$

$$\left.\frac{\partial C_s}{\partial r}\right|_{r=R_s} = -\frac{j_{Li}}{D_s} \tag{46}$$

  However there is a problem in applying the boundary condition at the sphere center, this is due to the term $1/r$ that becomes undetermined when $r=0$. To avoid this problem we apply L'Hopital rule which leads us to:

$$\frac{\partial C_s}{\partial t} = \begin{cases} 3\dfrac{D_s}{R_s^2}\dfrac{\partial^2 C_s}{\partial r^2} & \text{if } r = 0 \\ \dfrac{D_s}{R_s^2}\left[\dfrac{\partial^2 C_s}{\partial r^2} + \dfrac{2}{r}\dfrac{\partial C_s}{\partial r}\right] & \text{if } r > 0 \end{cases} \quad \frac{\partial c_s}{\partial r} = 0 \frac{\partial c_s}{\partial r} = -\frac{j_{Li}}{D_s}$$

- Faradic process

  Faraday's laws relate current and mass. The majority of bibliography indicates that the conditions at the boundary of the electrodes are of null potential flux (Neumann problem, (Schiesser, 1991). This imposes a difficulty because the problem does not possess a unique solution, rather it presents a family of solutions. To avoid this problem we can transform the Neumann condition to a Dirichlet one. For this purpose we can use Faraday's law in its integrated form:

$$\frac{1}{F}\frac{d\mathbf{i}_2}{dx} = aj_{Li} \tag{47}$$

$$\mathbf{i}_2|_b - \mathbf{i}_2|_a = \int_a^b Faj_{Li}dx \tag{48}$$

- Ohm's law

  Null potential flux conditions (Doyle & Newman, 1996) are normally used. However to promote better convergence in the solution of the model, we decided to transform the Neumann conditions to Dirichlet ones.

- Electrolyte

  The potential in the electrolyte is solved for the three regions; the potential at the negative electrode can be fixed to grant the accomplishment of Faraday's laws, this is expressed as:

$$\phi_2 = \phi_{2,0} \tag{49}$$

  provided that:

$$\mathbf{i}_2|_b - \mathbf{i}_2|_a = \int_a^b Faj_{Li}(\phi_{2,0})dx \tag{50}$$

  Current density is not calculated in this model. However, it is easily demonstrated that in the separator region it is constant. Taking into account that in the electrolyte region, j_{Li} equals zero, Eq. (47) reduces to:

$$\frac{d\mathbf{i}_2}{dx} = 0 \tag{51}$$

$$\mathbf{i}_2 = constant \tag{52}$$

  As Ohm's law is conservative we have:

$$I = \mathbf{i}_1 + \mathbf{i}_2 \tag{53}$$

  Combining the current density conservation (Eq. (3)) and the fact that in the separator there is only electrolyte (which implies that $\mathbf{i}_1 = 0$) we have the following:

$$\mathbf{i}_2 = I \tag{54}$$

  Following the same logic, we have that in the current collectors all the current flows trough the solid phase, this is expressed as $\mathbf{i}_1 = I$ or in terms of $\mathbf{i}_2$; $\mathbf{i}_2 = 0$.

  Considering the negative electrode the condition reads as follows:

$$\int_0^{\delta_s} Faj_{Li}dx = \mathbf{i}_2|_{x=\delta_s} - \mathbf{i}_2|_{x=0} \tag{55}$$

  under the latter deductions it becomes:

$$\int_0^{\delta_s} Faj_{Li}dx = I \tag{56}$$

  For the positive electrode, we keep Neumann null flux condition.

- Electrodes

  The null flux can also be used as a boundary condition in the separator and the Ohm's law at the current collectors (Doyle & Newman, 1996). However it is more convenient to adopt the convention of the electrode potential (ϕ_1) equal to zero at the interface between the current collector and the negative electrode, by doing this the potential of the positive electrode equals the cell potential; we kept the other conditions unchanged. The mathematical expressions for this boundary conditions are:

$$\phi_1|_{x=0} = 0 \tag{57}$$

$$\frac{d\phi_1}{dx}|_{x=\delta_s} = 0 \tag{58}$$

  For the positive electrode we assume a similar condition as the ones used for the electrolyte potential and kept Ohm's law at the current collector potential (Doyle & Newman, 1996):

$$\phi_1|_{x=\delta_a+\delta_s} = \phi_{1,0} \tag{59}$$

Table 2
Summary of boundary conditions.

Equation	$x=0$	$x=\delta_a$	$x=\delta_a+\delta_s$	$x=L$
Li+ diffusion [a]	$\frac{\partial c}{\partial x}=0$	Continuity	Continuity	$\frac{\partial c}{\partial x}=0$
Ohm's law [a]	$\phi_2=\phi_{2,0}$	Continuity	Continuity	$\frac{\partial \phi_2}{\partial x}=0$
Ohm's law [b]	$\phi_1=0$	$\frac{d\phi_1}{dx}=0$	$\phi_1=\phi_{1,0}$	$\frac{d\phi_1}{dx}=-\frac{I}{\sigma}$
Equation	$r=0$	$r=R_s$		
Li+ diffusion [b]	$\frac{\partial c_s}{\partial r}=0$	$\frac{\partial c_s}{\partial r}=-\frac{j_{Li}}{D_s}$		

[a] Electrolyte.
[b] Electrodes.

provided that:

$$\int_{\delta_a+\delta_s}^{L} Faj_{Li}(\phi_{1,0})dx = -I \tag{60}$$

$$\left.\frac{d\phi_1}{dx}\right|_{x=L} = -\frac{I}{\sigma} \tag{61}$$

Table 2 presents a summary of all boundary conditions within the anode, separator and cathode regions.

3. Model summary

The simplified and dimensionless model and respective boundary conditions are presented in Table 3. It constitutes a system of Partial Differential and Algebraic Equations. The boundary conditions are also presented. Notice that only c and ϕ_2 feature a continuity condition, but ϕ_1 does not.

4. Discretization

There are different approaches to solve partial differential equation systems. Probably the best well known are finite differences and finite volume. The basic idea behind these methods consists in providing an algebraic approximation to the differential terms in some or all the variables. The method of lines (MOL), lies under the same basic principle of substituting the spatial variables and keeping the first derivative in time, and rely on sophisticated solvers for the ordinary differential equations system obtained after discretization. In more specific cases, a system of partial and ordinary differential equations becomes a differential and algebraic equation system (DAEs).

Discretization is made by means of Taylor approximation and a series of algebraic manipulation. There are many types of discretization depending mainly on the number of discretized points and the degree of the derivative term; there are also some special types of discretization, for example the ones used to avoid fluctuations in the convective term. Because partial differential equations featuring convective and diffusive terms tend to be hard to be solved by numerical integration techniques, different manners of approximating the embedded first and second derivatives should be used. Therefore, in this work two discretization routines were used: dss010 (a 11 point, first order derivative discretization routine) and dss044 (a three point, second order derivative which can accept Dirichlet or Neumann type boundary conditions for the left and right boundaries). More information is available in Schiesser (1991).

The diffusion into the porous electrodes presents a pseudo-2-dimension problem, accounting for the spatial coordinate x and the spherical coordinate r of the active material sphere. It was necessary a gathering of variables leading to two matrices of dimension $np_a \times np_p$ and $np_c \times np_p$ for each electrode, where np_a and np_c are the number of points of discretization in each electrode and np_p is the number of discretized points in the spherical particles. After some trials we came to the conclusion that 11 points were enough for representing the system behavior for the three regions. The resulting system of DAEs was solved using the ode15i solver embedded in `Matlab`, which is an implicit solver. Other solvers where tested but this specific problem presented a considerable dependence between variables and could only be initialized with implicit solvers. The previous mentioned dependence between variables makes it hard for some solvers to achieve a consistent initialization, the approach we adopted was modified from previous works (Boovaragavan & Subramanian, 2011). Although each variable is solidly interconnected to the others, the ones that present the highest dependence are j_{Li}, ϕ_1 and ϕ_2. We first solved these three variables in their algebraic form for $t=0$ assuming all the concentrations equal to their initial values provided by the user, and then feed this vector corresponding to y_0 along with a vector of zeros with equal size that corresponds to y_0'. The equations corresponding to the three more dependent variables will be solved numerous times as time moves forward in the solver, but now with varying concentrations in the electrodes and electrolyte. The complete Matlab code can be consulted elsewhere (Martinez-Rosas, 2010).

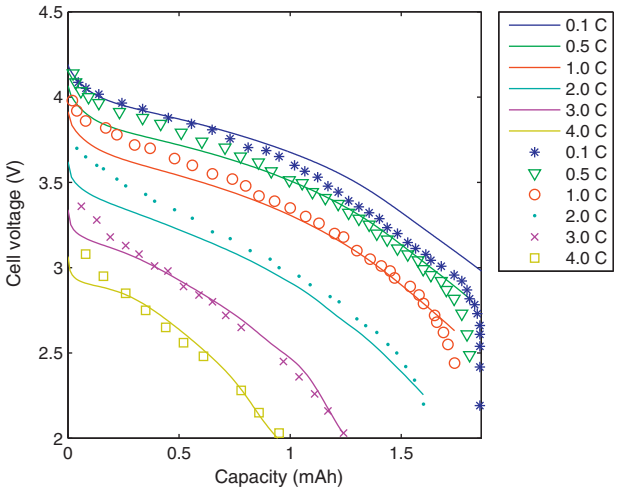

Fig. 2. Comparison between simulated (continuous line) and experimental (discontinuous points) data for different values of the discharge rate.

5. Experimental validation

The results obtained from Matlab simulations were compared versus experimental data (Doyle & Newman, 1996). The agreement between simulated and experimental data is presented in Fig. 2. A film resistance coefficient was proposed in the same work to promote a better concordance and somehow explain the formation of undesirable compounds in the electrodes. The same coefficient value ($R_f = 900\Omega/cm^2$) was used in the anode side. The over-potential equation is modified as follows:

$$\eta_a = \phi_1 - \phi_2 - u^o - Fj_{Li}R_f$$

Fig. 2 presents the comparative values of experimental and simulated data for different discharge rates in C notation (1.0 C is the current that exhaust the battery to its cut-off voltage in 1 h). Percentage errors are presented in Fig. 3. It can be noticed that the majority of these errors lies between ±5% of the real value, which is considered an acceptable error.

6. Base simulation

In this part we compare the results obtained using our model against other published results (Doyle et al., 1993). We claim that

Table 3
Summary of the mathematical model.

Governing equation	Boundary condition	
Anode	$x=0$	$x=\delta_a$
$\epsilon\frac{\partial c}{\partial t}=\frac{D}{\delta^2}\frac{\partial^2 c}{\partial x^2}+a(1-t_+^o)j_{Li}$	$\frac{\partial c}{\partial x}=0$	Continuity
$-\frac{\sigma}{\delta^2}\frac{\partial^2\phi_1}{\partial x^2}=-Faj_{Li}$	$\phi_1=0$	$\frac{d\phi_1}{dx}=0$
$-\frac{\kappa}{\delta^2}\frac{\partial^2\phi_2}{\partial x^2}=Faj_{Li}+\frac{2\kappa RT}{\delta^2 F}\left(1-t_+^o\right)\frac{\partial^2 \ln c}{\partial x^2}$	$\phi_2=\phi_{2,0}$	Continuity
Separator	$x=\delta_a$	$x=\delta_a+\delta_s$
$\frac{\partial c}{\partial t}=\frac{D}{\delta^2}\frac{\partial^2 c}{\partial x^2}$	Continuity	Continuity
$-\frac{\kappa}{\delta^2}\frac{\partial^2\phi_2}{\partial x^2}=Faj_{Li}+\frac{2\kappa RT}{\delta^2 F}\left(1-t_+^o\right)\frac{\partial^2 \ln c}{\partial x^2}$	Continuity	Continuity
Cathode	$x=\delta_a+\delta_s$	$x=L$
$\epsilon\frac{\partial c}{\partial t}=\frac{D}{\delta^2}\frac{\partial^2 c}{\partial x^2}+a(1-t_+^o)j_{Li}$	Continuity	$\frac{\partial c}{\partial x}=0$
$-\frac{\sigma}{\delta^2}\frac{\partial^2\phi_1}{\partial x^2}=-Faj_{Li}$	$\phi_1=\phi_{1,0}$	$\frac{d\phi_1}{dx}=-\frac{I}{\sigma}$
$-\frac{\kappa}{\delta^2}\frac{\partial^2\phi_2}{\partial x^2}=Faj_{Li}+\frac{2\kappa RT}{\delta^2 F}\left(1-t_+^o\right)\frac{\partial^2 \ln c}{\partial x^2}$	Continuity	$\frac{\phi_2}{\partial x}=0$
Active material (anode and cathode)	$r=0$	$r=R_s$
$\frac{\partial C_s}{\partial t}=\begin{cases}3\frac{D_s}{R_s^2}\frac{\partial^2 C_s}{\partial r^2} & \text{if } r=0\\ \frac{D_s}{R_s^2}\left[\frac{\partial^2 C_s}{\partial r^2}+\frac{2}{r}\frac{\partial C_s}{\partial r}\right] & \text{if } r>0\end{cases}$	$\frac{\partial c_s}{\partial r}=0$	$\frac{\partial c_s}{\partial r}=-\frac{j_{Li}}{D_s}$
Auxiliary equations		
$\eta=\phi_1-\phi_2-u^o$	$j_n=i_o\left\{\exp\left(\frac{F}{2RT(\eta-U^o)}\right)-\exp\left(\frac{-F}{2RT(\eta-U^o)}\right)\right\}$	
$\int_0^{\delta_s}Faj_{Li}(\phi_{2,0})dx=I$	$\int_{\delta_a+\delta_s}^{L}Faj_{Li}(\phi_{1,0})dx=-I$	

our results are in good agreement with expected results and outperform previous reported solutions. The base case of the simulation was the one simulated by Doyle et al. (1993). The thermodynamic, kinetic and transport parameters as well as the design variables are presented in Table 4. The variables computed are:

- Anodic and cathodic Potentials ($\phi_1^{a,c}$).
- Electrolyte potential (three regions) ($\phi_2^{a,s,c}$).
- Li-ion flux in the electrodes ($j_{Li}^{a,c}$).
- Li-ion concentration in the electrolyte ($C_e^{a,s,c}$).
- Li-ion concentration in the both active materials ($C_s^{a,c}$).

The electrode potentials are presented in Fig. 4. It can be noticed that the electrodes are practically equipotential surfaces. This is of interest given the fact that they are not metallic plates but porous 3-D materials. Also the anodic potential remains almost constant. This fact allows us to calculate the cell potential (V_{cell}) as the cathodic potential in the interface with the current collector. This fact is not a coincidence, since we previously fixed the anodic potential at its interface with the current collector to zero.

Potential values of the electrolyte are shown in Fig. 5. Electrolyte potential values grow in absolute value as discharge occurs. This

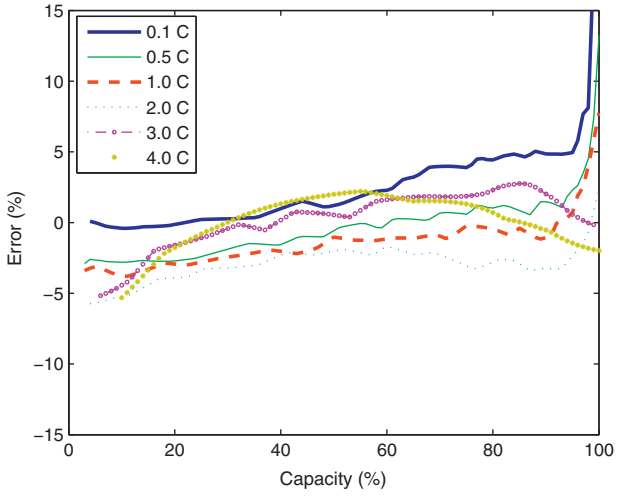

Fig. 3. Percentage errors of the simulation

Table 4
Parameters of the base simulation (all from Doyle and Newman (1996)).

Parameters	Description	Value
Operation variables		
I	Discharge current (1.0 C)	17.5 A/m^2
T	Temperature	298 K
Design variables		
$C_{e,0}$	Initial concentration of $LiPF_6$ in the electrolyte	2000 mol/m^3
$C_{sa,0}$	Initial concentration of Li ions in the anode	14,870 mol/m^3
$C_{sc,0}$	Initial concentration of Li ions in the cathode	3900 mol/m^3
δ_a	Anode width	100 μm
δ_c	Cathode width	174 μm
δ_s	Separator width	52 μm
ε_a	Anode porosity	0.357
ε_c	Cathode porosity	0.444
Kinetic, thermodynamic and transport parameters		
C_T^a	Max. conc. of Li ions in the anode	26,390 mol/m^3
C_T^c	Max. conc. of Li ions in the cathode	22,860 mol/m^3
D_s^a	Particle diffusivity coefficient in the anode	3.9×10^{-14} m^2/s
D_s^c	Particle diffusivity coefficient in the cathode	1.0×10^{-13} m^2/s
D	Electrolyte diffusivity coefficient	7.5×10^{-11} m^2/s
k_r^a	Reaction rate constant in the anode	2×10^{-11} m$^{5.5}$/mol$^{0.5}$ s
k_r^c	Reaction rate constant in the cathode	2×10^{-11} m$^{5.5}$/mol$^{0.5}$ s
R_p^a	Radius of the active material sphere in the anode	12.5 μm
R_p^c	Radius of the active material sphere in the cathode	8.5 μm
t_+^o	Transport number	0.363
σ^a	Conductivity in the anode	100 S/m^2
σ^c	Conductivity in the cathode	3.8 S/m^2
	Description	Formula
Calculated parameters		
$a^{a,c}$	Specific area of the electrodes (m^2/m^3)	$3\frac{\varepsilon_s}{R_p}$
ε_s^a	Volume fraction of the solid phase in the anode	$1-\varepsilon^a-0.172$
ε_s^c	Volume fraction of the solid phase in the cathode	$1-\varepsilon^c-0.259$

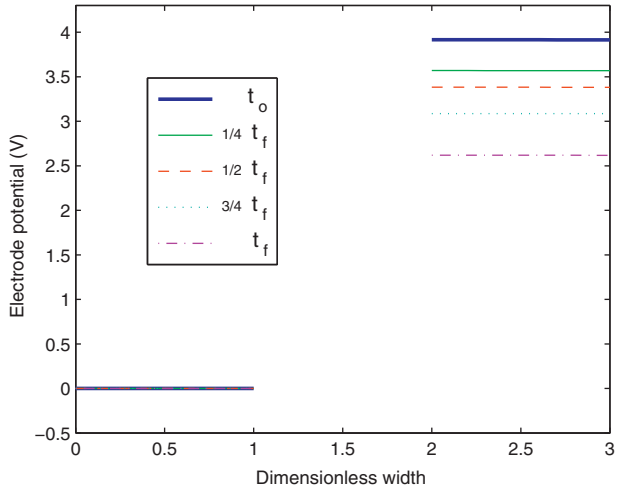

Fig. 4. Electrode potentials (ϕ_1), anodic (left) and cathodic (right).

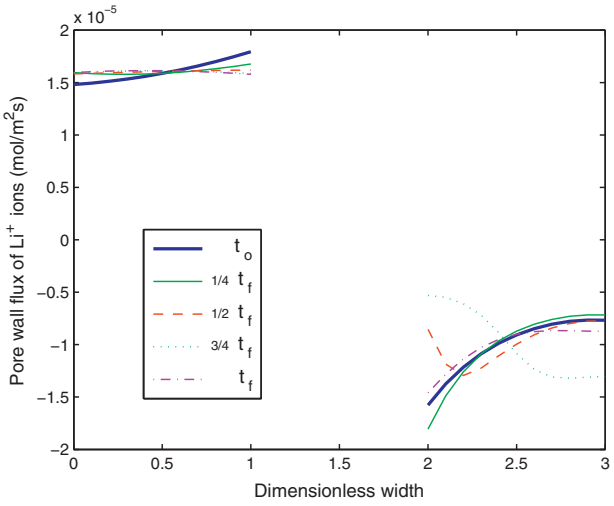

Fig. 6. Li-ion flux in the electrodes (j_{Li}).

effect can be attributed mainly to the emergence of the concentration gradient. If we had chosen to use the dilute theory instead of the concentrated theory, this phenomenon would not have been observed adequately (Doyle & Newman, 1996).

The pore-wall flux of lithium ions in the electrodes is shown in Fig. 6. In the anode side this variable does not change considerably. For the cathode we can see some quasi-stability followed by a transition period after which quasi-stability is achieved once more. This variable is considered to be the more important of the model (Boovaragavan & Subramanian, 2011), due to the level of interdependence with respect to the other variables both implicit and explicit ($j_{Li} = (c, c_s, \eta)$) and is also present in virtually all equations (9 out of 10).

Lithium-ions concentration in the electrolyte is presented in Fig. 7. The results obtained in this work are considerably different from those reported by Doyle and Newman (1996). Nevertheless, the ones presented in this work are more realistic somehow that the latter, which present zones of constant concentration along the time, while our solution presents a continuous evolution without constant points. This phenomenon can be explained by the treatment given to the concentration of lithium ions in the electrolyte as a continuum across the three regions. For this effect we consider vectors of the specific parameters (a, D^{eff}, $\varepsilon and \delta_i$) of each region.

Concentration of lithium ions in the electrodes is presented in Fig. 8. The zig-zag shape or discontinuities represents two pseudo-

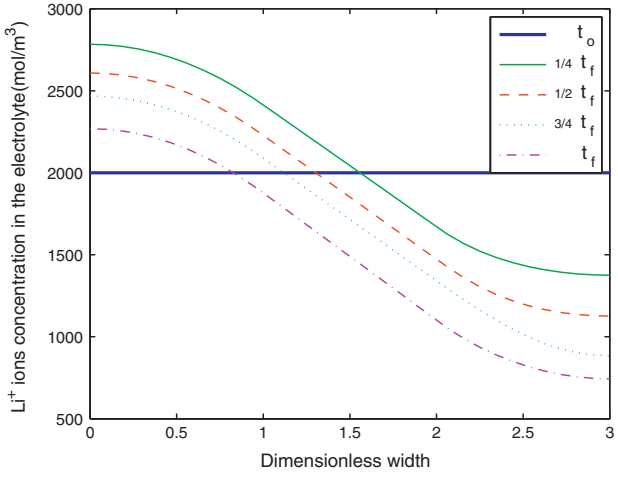

Fig. 7. Li-ion concentration in the electrolyte (C_e).

dimensions; r dimension of spherical particles, and x dimension corresponding to the cells width. In this way, each section of the curve represents the behavior inward the particle of a single x discretized point. Figure shows 121 discretized points (11

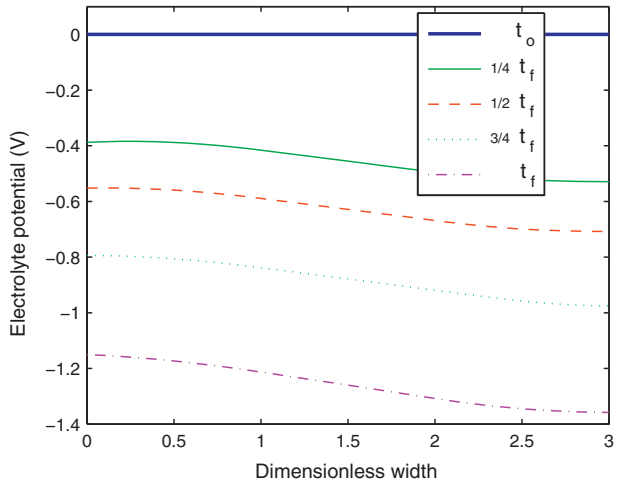

Fig. 5. Electrolyte potential (ϕ_2).

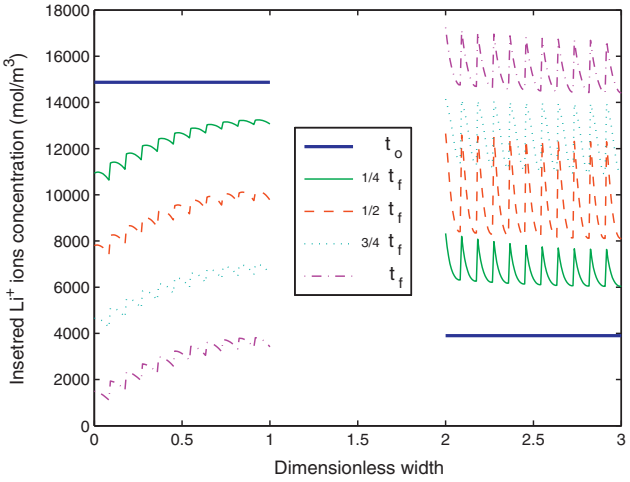

Fig. 8. Li ions concentration in the electrodes (C_s).

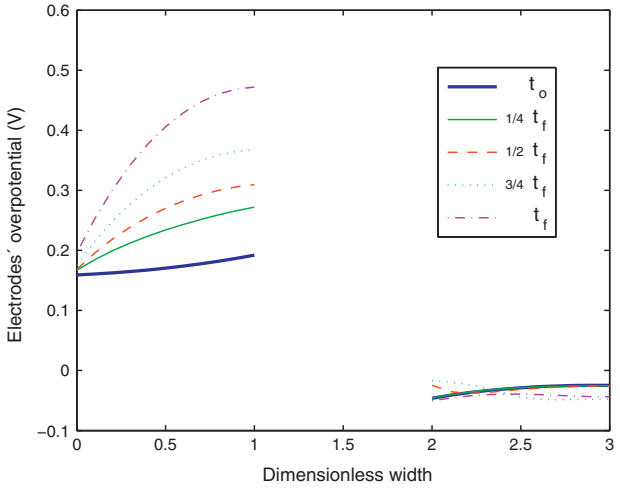

Fig. 9. Over-potential (η).

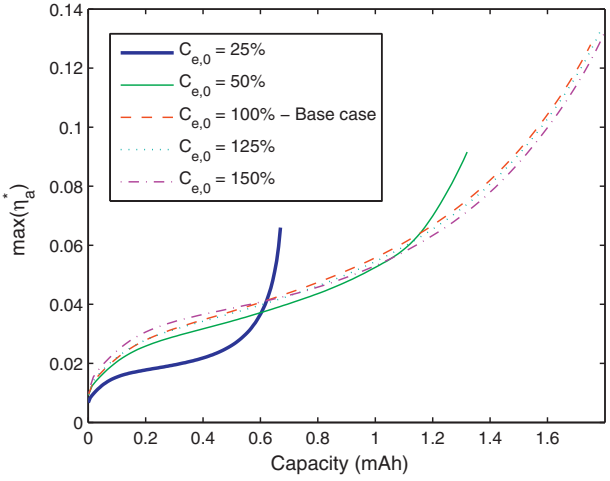

Fig. 10. Variation of the parameter $C_{e,0}$.

points in x-direction × 11 points in r-direction), for each electrode. Much of the computational effort is dedicated to the solution of the electrodes concentration (242 variables of the 354 calculated). Information from insertion and extraction is crucial to the calculation of the performance of the cell, and provides the degree of charge (DOC), that indicates the amount of available energy in the battery, that is difficult to estimate in any other way. Although there are algebraic and differential approximations to the diffusion equation (Zhang & White, 2007) that would eliminate the r sub-dimension, these approximations introduce a significant error, considering the amplification of the error for the whole model. Applying exact equations, instead of approximations requires a balance between discretized points in r and in x directions. Previous tests with increased number of r points, resulted in a non convergence problem of the calculations mainly because of stiffness issues. Simplified attempts, increasing the number of points from 11 to 20 did not alter the results significantly. This demonstrates that MOL efficiency is achieved even with few points. Electrode over-potentials (calculated in the post-processing) is presented in Fig. 9. This variable was not calculated explicitly because is not strictly necessary to calculate other variables.

7. Case studies

After carrying out validation of our model against both experimental information and published results, we use the model to explore some potential and practical applications of Li-ion dynamic battery models. First we present some sensibility results by changing some important design parameters. Then, we explore the dynamic performance of the Li-ion battery by carrying out some tests whose aim is to demonstrate the battery performance under different driving scenarios. Finally, because battery performance can be improved by using different battery arrangements, we explore a parallel battery connection.

7.1. Simulation of the variation in the design parameters

The performance of different Li-ion batteries is studied by varying the design parameters. The parameters chosen for this analysis where:

- $C_{e,0}$: initial concentration of the salt in the electrolyte,
- $\delta^{a,c}$: electrodes width,
- $\varepsilon^{a,c}$: electrodes porosity

For the simulations the next scenario was considered. The nominal capacity of the battery was found. Each battery was discharged at a 1.0 C-rate to a cutoff voltage of 2.6 V. The maximum dimensionless anodic over-potential was used as a measure of stress of the battery according to the following equation:

$$\eta_a^* = \frac{\eta_a}{V}$$

- **Li-ion initial concentration in the electrolyte**

  The concentration of the Li-ions in the electrolyte affects its conductivity (κ) in a non-linear way. The parameter $C_{e,0}$ was varied in a range between 25 and 150% of its base value. Fig. 10 shows the over-potential and capacity of batteries with different initial concentration of the Li ion in the electrolyte. It can be seen that a battery with an initial condition under 2000 mol/m^3 gives rise to a low capacity battery (∼0.6 mAh/m^2). On the other hand, above this concentration the increase in the capacity of the cell is minor (1.65–1.8 mAh/m^2). Then, we can conclude that this variable is susceptible of optimization, especially when considering that the electrolyte salt represents a considerable percentage of the battery manufacture cost.
- Electrodes width

  The electrodes width determines two main factors in the operation of the battery: the amount of active material and the resistance to the mass transport. The width of both electrodes was varied uniformly in a range between 80 to 120 % of the base value. The results are shown in Fig. 11. In this case we found a slight increase in battery capacity when the electrode width increases.
- Electrodes porosity

  The porosity of the electrodes affects the effective conductivity of the electrolyte and is also a resistance to the mass transference process. The variation of these variables was made in the same range as that of the widths. Results are presented in Fig. 12. As the relation is non-linear, there is an opportunity for optimization of this parameter.

7.2. Simulation of the dynamic operation of the battery

Dynamic operation refers to the changes in operating conditions, being these the discharge rate and temperature. The model does not consider the dynamic changes in temperature, so that only changes in current are analyzed.

Electrical vehicles the same as internal combustion engines, are subject to different driving regimes. The broader classification

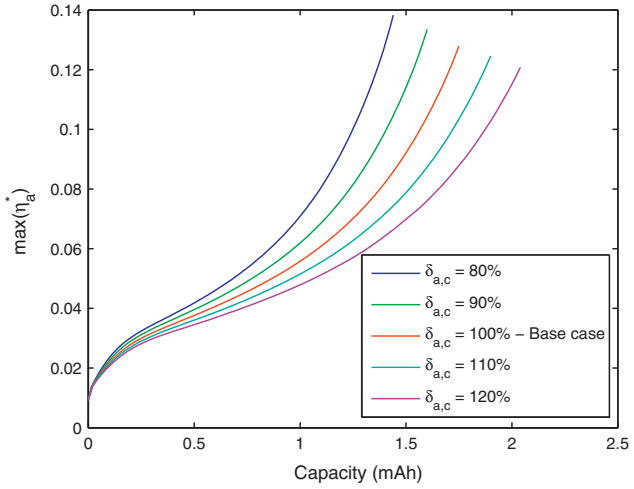

Fig. 11. Variation of the parameter $\delta^{a,c}$.

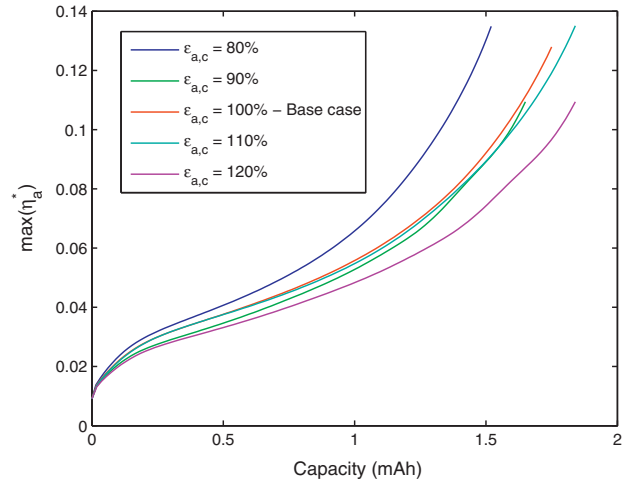

Fig. 12. Variation of the parameter $\varepsilon_{a,c}$.

divides them into city and suburban regimes. The city regime is characterized by repetitive cycles of acceleration and braking. On the other hand, the suburban regime presents longer periods of acceleration and deceleration with minimal full stops. The regime affects the performance and duration of the battery in the same way as the fuel performance (i.e. km/gal) for the internal combustion vehicles. The city regime includes short periods of acceleration and braking. An idealized scheme is presented in Table 5. The simulation of this regime is presented in Fig. 13. The suburban regime

Table 5
Dynamic operation in city regime.

I (C/m^2)	Time (s)	Description
1.00	5	Start
0.25	10	Disacceleration
−0.25	7	Braking
0.00	10	Full stop
1.80	10	Acceleration
0.60	30	Disacceleration
−0.50	12	Braking
0.00	15	Full stop
2.20	25	Acceleration
0.90	10	Disacceleration
−0.60	10	Braking
0.50	20	Acceleration
0.00	10	Full stop

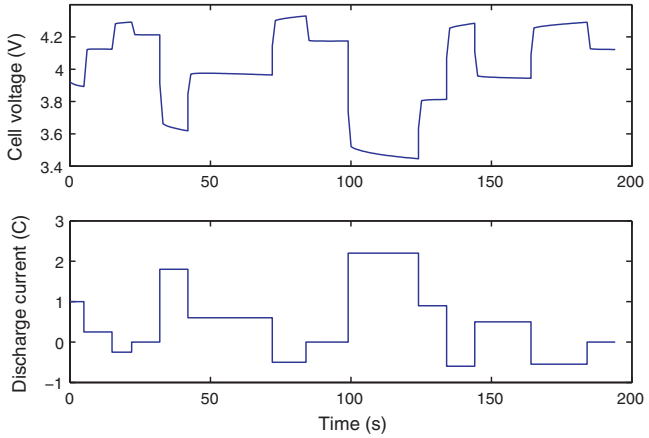

Fig. 13. Simulation of a battery in city regime.

Table 6
Dynamic operation in suburban regime.

I (C/m^2)	Time (s)	Description
3.00	60	Start
2.00	60	Disacceleration
−1.50	10	Braking
1.00	60	Acceleration
3.80	25	Vigorous acceleration
1.00	50	Disacceleration
4.00	50	Vigorous acceleration
3.20	120	Full stop
−2.00	20	Braking
0.00	25	Full stop

is characterized by longer periods of acceleration and deceleration, some braking and virtually no full stops. A representation of this scheme is shown in Table 6. The voltage profile under the suburban regime is presented in Fig. 14

7.3. Parallel batteries simulation

Series and parallel arrangements of batteries are used to increase the voltage and capacity of the system. However these arrangements may present problems due to the lack of equalization of the batteries. This refers to the different rates of discharge that each battery is subject to and their states of charge are also different. One application of interest is to enhance the electric vehicle battery performance by the construction of an arrangement of different capacity batteries in parallel (Wu, Lin, Wang, Wan, & Yang, 2006).

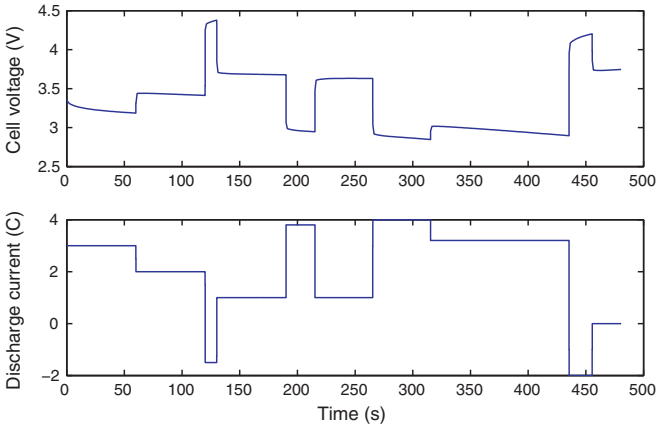

Fig. 14. Simulation of a battery in a suburban regime.

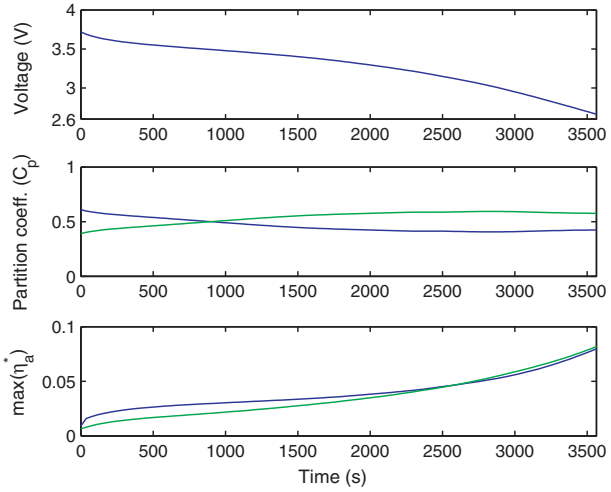

Fig. 15. Simulation of batteries in parallel.

The basic idea is to connect a high energy density battery to a high power density one, expecting that the system would respond adequately to peak demands of current and also have a long discharge time.

We present two criteria for simulation:

- The total discharge current is equal to the sum of the individual batteries.
- The voltage of both batteries remains equal at all times.

These conditions come from the basic theory of parallel circuits. A simulation that fulfills both restrictions is proposed under the following considerations: both batteries are solved as a coupled system; a term that relates the total current to the individual currents is created and named partition coefficient, is calculated in the simulation with the restriction of having equal voltages in both batteries.

A simulation was carried out with the base case battery and the one of augmented width of 20%. The nominal capacities of both batteries are 17.5 and 20.4 Ah/m^2 respectively. The expected capacity of the arrangement is 37.9 Ah/m^2. Fig. 15 shows the results of the simulation at 1.0 C-rate (37.9 Ah) of the parallel arrangement.

8. Conclusions

Fossil fuels have been for many years the main source of energy supply for many applications including the transportation sector. There are now some evidences that this strong dependence on fossil fuels is one of the main reasons for climatic change problems and urban pollution. Moreover, it has been predicted that soon world scale oil exploitation will reach its maximum peak. Therefore, there is a real need to explore the use of alternative sustainable energy sources able to meet our energy demands. It is certainly true that none of the new alternative energies being considered (i.e. biofuels, fuel cells, batteries, wind and solar power, etc) by themselves will be capable of meeting world scale energy demands. What we require is the integration of all these alternative energies with conventional fossil fuels (during the transition period from fossil fuels energy to alternative energies) (Weekman, 2010). Therefore, in this work our aim was to explore the use of advanced energy storage devices (Li-ion batteries) to partially meet future energy demands. Although there is a great number of published works dealing with the chemistry of Li-ion batteries, few works have addressed the modeling and simulation of Li-ion batteries to explore process sensitivity and their dynamic performance during different driving scenarios. Hence, the modeling and simulation of the Li-ion batteries with chemistry Li_xC_6−− $Li_yMn_2O_4$ were addressed in the present work. The model used was modified from that of Doyle et al Doyle and Newman (1996) in the boundary conditions. The MOL was used in the discretization of the system into a DAE system. A program in the form of a Matlab function was developed for the simulation of the battery and the calculation of electrochemical variables. The mathematical model was experimentally validated and tested with different applications. These include the variation of design parameters, the dynamic operation of batteries and the simulation of different capacity batteries connected in parallel. Simulation with design purposes and the prediction of the degree of discharge are the following steps in the line of investigation proposed by this work as well as the integration of the temperature dependence. Future work includes the determination of optimal control policies to maximize the performance of Li-ion batteries. With the advent of powerful CPU processors and advances in non-linear predictive control techniques (Zavala & Biegler, 2009; Huang, Zavala, & Biegler, 2009) it may be feasible to address the real time implementation of those optimal control policies.

References

Baker, D. R., & Verbrugge, M. W. (1999). Temperature and current distribution in thin-film batteries. *Journal of the Electrochemical Society*, *146*(7), 2413–2424.

Boovaragavan, V., & Subramanian, V. R. (2007). A quick and efficient method for consistent initialization of battery models. *Electrochemistry Communications*, *9*(7), 1772–1777.

Broussely, M., & Archdale, G. (2004). Li-ion batteries and portable power source prospects for the next 5–10 years. *Journal of Power Sources*, *136*, 386–394.

Cairns, E. J., & Albertus, P. (2010). Batteries for electric and hybrid-electric vehicles. *Annual Review of Chemical and Biomolecular Engineering*, *1*, 299–320.

Chung, G. C., Jun, S. H., Lee, K.-Y., & Kim, M. H. (1999). Effect of surface structure on the irreversible capacity of various graphitic carbon electrodes. *Journal of the Electrochemical Society*, *146*, 1664–1671.

Delmas, C., & Saadoune, I. (1992). Electrochemical and physical properties of the $Li_xNi_{1-y}Co_yO_2$ phases. *Solid State Ionics*, *53–56*, 370–375.

Doyle, M., Fuller, T. F., & Newman, J. (1993). Modeling of the galvanostatic charge and discharge of te lithium/polymer/insertion cell. *Journal of the Electrochemical Society*, *140*(6), 1526–1533.

Doyle, M., & Newman, J. (1903). Comparison of the modeling predictions with experimental data from plastic lithium ion cells. *Journal of the Electrochemical Society*, *143*(6), 1890.

Fuller, T. F., Doyle, M., & Newman, J. (1994). Simulation and optimization of the dual lithium ion insertion cell. *Journal of the Electrochemical Society*, *141*(1), 1–10.

Garca, R. E., & Chiang, Y.-M. (2007). Saptially resolved modeling of microstructurally complex battery architectures. *Journal of the Electrochemical Society*, *154*(9), A856–A864.

Huang, R., Zavala, V. M., & Biegler, L. T. (2009). Advanced step nonlinear model predictive control for air separation units. *Journal of Process Control*, *19*(4), 678–685.

Huggins, R. A. (2009). *Advanced batteries: Materials sciences aspects*. Springer.

Linden, D., & Reddy, T. B. (2002). *Handbook of batteries* (3rd. ed.). McGraw-Hill.

Liaw, B. Y., Jungst, R. G., & Nagasubramanian, G. (2005). Modeling capacity fade in lithium-ion cells. *Journal of Power Sources*, *140*(1), 157–161.

Michio, I. (1996). Carbon materials structure, texture and intercalation. *Solid state ionics*, *86–88*, 833–839.

Martinez-Rosas, E. (2010). Modeling and simulation of lithium-ion batteries (in Spanish), M.Sc. Thesis, UNAM, México.

Newman, J., & Thomas-Alyea, K. (2004). *Electrochemical systems*. John Wiley & Sons, Inc.

Ning, G., & Popov, B. N. (2004). Cycle life modeling of lithium-ion batteries. *Journal of the Electrochemical Society*, *151*, A1584–A1591.

Ozawa, K. (1994). Lithium-ion rechargeable batteries with $LiCoO_2$ and carbon electrodes - the $LiCoO_2$/C system. *Solid State Ionics*, *69*, 212–221.

Schiesser, W. E. (1991). *The numerical method of lines: Integration of partial differential equations*. Academic Press.

Scrosati, B., & Grache, J. (2010). Lithium batteries: Status, prospectus and future. *Journal of Power Sources*, *195*(9), 2419–2430.

Seung-Taek, M., Atsushi, O., Ki-Soo, L., Shinichi, K., Yang-Kook, S., & Hitoshi, Y. (2008). Structural electrochemical, and thermal aspects of $Li[(Ni_{0.5}Mn_{0.5})_{1-x}Co_x]O_2$ ($0 \leq x \leq 0.2$) for high-voltage application of lithium-ion secondary batteries. *Journal of the Electrochemical Society*, *155*, A374–A383.

Shina, J.-H., Basak, P., Kerr, J. B., & Cairns, E. J. (2008). Rechargeable Li/$LiFePo_4$ cells using N-methyl-N-butyl pyrrolidinium bis(trifluoromethane

sulfonyl)imidelitfsi electrolyte incorporating polymer additives. *Electrochimica Acta*, *54*, 410–414.

Tang, M., Albertus, P., & Newmana, J. (2009). Two-dimensional modeling of lithium deposition during cell charging. *Journal of the Electrochemical Society*, *155*, A390–A399.

Tran, T. D., Spellman, L. M., Pekala, R. W., Goldberger, W. M., & Kinoshita, K. (1995). Graphitized needle cokes and natural graphites for lithium intercalation. *Journal of the Electrochemical Society*, *142*, 3297.

Wang, G. X., Bradhurst, D. H., Dou, S. X., & Liu, H. K. (1998). Structural and electrochemical characteristics of $Li_{1+x}Mn_{2-x}O_4$ and $LiMn_2O_{4-\delta}$ for Secondary Lithium batteries. In *Battery Conference on Applications and Advances, 1998., The Thirteenth Annual* Long Beach, CA, USA, (pp. 375–380). doi:10.1109/BCAA.1998.653898

Weekman, V. W. (2010). Gazing into an energy cristall ball. *Chemical Engineering Progress*, *106*(6), 23–27.

Whittingham, M. S. (2004). Lithium batteries and cathode materials. *Chemical Reviews*, *104*, 4271–4302.

Wu, M.-S., Lin, C.-Y., Wang, Y.-Y., Wan, C.-C., & Yang, C. R. (2006). Numerical simulation for the discharge behaviors of batteries in series and/or parallel-connected battery pack. *Electrochimica Acta*, *52*, 1349–1357.

Wu, J., Srinvasan, V., Xu, J., & Wang, C. Y. (2002). Newton Krylov multigrid algorithms for battery simulation. *Journal of the Electrochemical Society*, *149*(10), A1342–A1348.

Zavala, V. M., & Biegler, L. T. (2009). ptimization-based strategies for the operation of low-density polyethylene tubular reactors: Nonlinear model predictive control. *Computers and Chemical Engineering*, *33*(10), 1735–1746.

Zhang, Q., & White, R. E. (2007). Comparison of approximate solution methods for the solid phase diffusion equation in a porous electrode model. *Journal of Power Sources*, *165*, 880–886.